



Samipour, A., Dideban, D. and Heidari, H. (2019) First principles study of the ambipolarity in a germanene nanoribbon tunneling field effect transistor. *ECS Journal of Solid State Science and Technology*, 8(12), M111-M117. (doi:10.1149/2.0021912jss)

There may be differences between this version and the published version. You are advised to consult the publisher's version if you wish to cite from it.

<http://eprints.gla.ac.uk/203631/>

Deposited on: 18 November 2019

Enlighten – Research publications by members of the University of Glasgow
<http://eprints.gla.ac.uk>

1 First principles study of the ambipolarity in a germanene nanoribbon 2 tunneling field effect transistor

3 Azam Samipour¹, Daryoosh Dideban^{1,*}, Hadi Heidari²

4 ¹Institute of Nanoscience and Nanotechnology, University of Kashan, Kashan, Iran

5 ²James Watt School of Engineering, University of Glasgow, G12 8QQ, Glasgow, United Kingdom

6 * Corresponding author email: dideban@kashanu.ac.ir

7 8 **Abstract**

9 In this article, the effects of hetero-dielectric gate material and gate-drain underlap
10 on the ambipolar and ON-state current of a germanene nanoribbon (GeNR)
11 tunneling field-effect transistors (TFETs) is examined. The simulations are
12 performed using the combination of density functional theory (DFT) and non-
13 equilibrium Green's function (NEGF) formalis

14
15 m. It was observed that using high-k dielectric gate material increases the ON-state
16 current while the combination of hetero-dielectric gate material and gate-drain
17 underlap suppresses the ambipolar current and improves the ON-state current. In
18 addition, the effect of various hetero-junctions in the source region on the
19 performance of GeNR-TFET was investigated. Due to the dependency between the
20 width and energy bandgap in GeNR, utilizing a small bandgap in the source
21 improves ON-state current and its ambipolar behavior.

22
23 **Keywords:** 2D materials; germanene nanoribbon; tunneling field-effect transistor;
24 hetero-gate dielectric; gate-drain underlap; heterojunction.

25 26 **1. Introduction**

27 In order to continue performance improvement of Metal-Oxide-Semiconductor
28 field effect transistors (MOSFETs), their dimensions have been scaled down
29 continuously in the last decades and it is reached to less than 10 nm now. However,
30 this matter has led to a significant increase in power consumption. Due to
31 aggressive shrinking of the device dimensions, short-channel effects such as drain
32 induced barrier lowering (DIBL) are increased resulting in worse leakage current.
33 On the other hand, the fundamental theoretical limit of the subthreshold swing
34 (SS), which is about 60 mV/dec at room temperature for conventional MOSFETs,
35 does not permit further decrease of the leakage current in these devices. Therefore

36 alternative device structures and materials are proposed to overcome these
37 problems[1-7]. They could offer a subthreshold swing (SS) smaller than 60
38 mV/dec[2]. In recent years special attention has been paid to novel 2D materials
39 and in particular to graphene, silicene and germanene because of their unique
40 electronic, mechanical and optical properties. They offer a great potential for future
41 nanoelectronic device applications[8-11].

42 These materials are two-dimensional with a hexagonal honeycomb structure. There
43 is a Dirac point and a linear electronic dispersion around this point in these
44 materials. They belong to group IV of the periodic table. Graphene is comprised of
45 sp^2 hybridized carbon atoms and planar configuration whereas silicene and
46 germanene because to the mixing of sp^2 and sp^3 hybridization have low-buckled
47 structure[10-18]. Various studies show that graphene, germanene and silicene
48 monolayers have zero bandgap. Since in electronic devices, semiconductor
49 materials with a tunable band gap is required it was necessary to overcome this
50 issue. Utilizing these materials as nanoribbons with a desired width yields a non-
51 zero bandgap which is tunable[8, 11, 12, 19-21]. Graphene, germanene and
52 silicene nanoribbons are candidates for next generation devices due to significant
53 electronic properties such as direct bandgap and light carrier effective mass[2, 22-
54 24], high carrier mobility and high current density[23, 25-27].

55 On the other hand, TFETs which are based on interband tunneling mechanism have
56 attracted much interest. TFETs have advantages such as subthreshold swing below
57 60mV/dec, less leakage current and better immunity to short channel effects
58 (SCEs). However, disadvantages are also observed, such as less on-current (I_{ON})
59 than a high performance MOSFET and ambipolar behavior in TFETs.
60 Ambipolarity means that depending on the type of voltage applied, tunneling
61 happens in two directions. In n-channel TFETs, for instance, by applying positive
62 gate voltage, electrons tunnel from the source to the channel that this results in an
63 on-state current (I_{ON}) while by applying a negative gate voltage, hole tunneling
64 occurs from the drain to the channel that results in an ambipolar current (I_{amb}).

65 This problem degrades the switching characteristics and makes the TFET less
66 efficient for digital circuit design. In order to overcome these issues, several
67 methods have been introduced. The most important among them are use of high-k
68 gate dielectric, multiple-gate structure, hetero-dielectric gate (HG), gate-drain
69 overlap, heterojunction TFETs, drain underlap, band-gap engineered TFETs and
70 drain doping engineering[28-36].

71 In this paper, the effect of hetero-dielectric and a gate-drain underlap on the
72 ambipolar characteristics and ON-state current in a GeNR-TFET is investigated.
73 Moreover, the effect of changing the source bandgap on the performance of this
74 device is evaluated.

76

77 **2. Device structure and simulation setup**

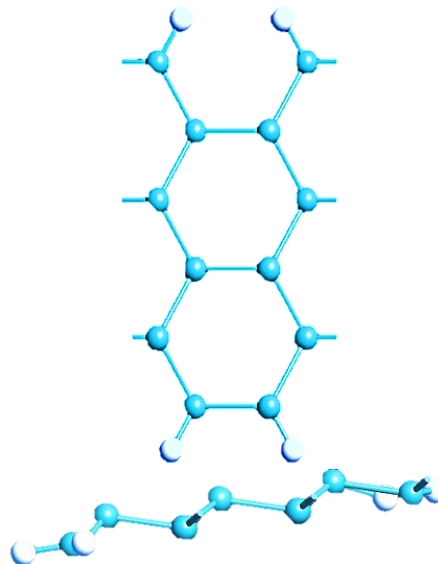
78 The electronic properties and current-voltage characteristics were investigated
79 utilizing the density functional theory (DFT) and non-equilibrium Green's function
80 (NEGF) method in the Atomistic ToolKit -Virtual Nanolab (ATK-VNL) [37].

81 The exchange correlation employed is the Generalized Gradient Approximation
82 (GGA) of Perdew–Burke–Ernzerhof (PBE) functional. The cutoff energy and a
83 Monkhorst-Pack k-point are considered 80 Hartree and $1 \times 1 \times 51$, respectively.
84 Hartwigsen–Goedecker–Hutter (HGH) pseudopotential is applied as basis set [10].

85 Periodic boundary conditions with vacuum layer of approximately 15 Å for each
86 side of the unitcell are employed to prevent undesired image-image interaction. It
87 is worth noting that the vacuum layer size for the AGeNR case is in agreement
88 with the previous works presented in [38, 39].

89 To remove the dangling bond effects on the surface of nanoribbons, edges on both
90 sides were passivated with hydrogen atoms. In order to obtain the optimum
91 structure, the initial defined structure is relaxed until the maximum atomic force to
92 each atom smaller than $0.02 \text{ eV}/\text{Å}$ is obtained. The $1 \times 1 \times 101$ k-points have been
93 used to obtain electronic properties. Moreover, the temperature is set at $T = 300$
94 K [10, 38]. Fig. 1 illustrates the armchair GeNR unit cell. The bond length of Ge–
95 Ge and parameter of buckling was obtained 2.4 Å and $\Delta = 0.67 \text{ Å}$, respectively.

96



97

98

99

Fig1: Top and side views of the relaxed 6-AGeNR.

100

101

102 I–V characteristic behavior under a drain-source voltage (V_{bias}) and gate voltage

103 (V_g) is calculated as:

104

$$I(V_g, V_{bias}) = \frac{2e}{h} \int_{-\infty}^{+\infty} \{ Tr[\Gamma_L G^R \Gamma_R G^A] [f_L(E - \mu_L) - f_R(E - \mu_R)] \} dE \quad (1)$$

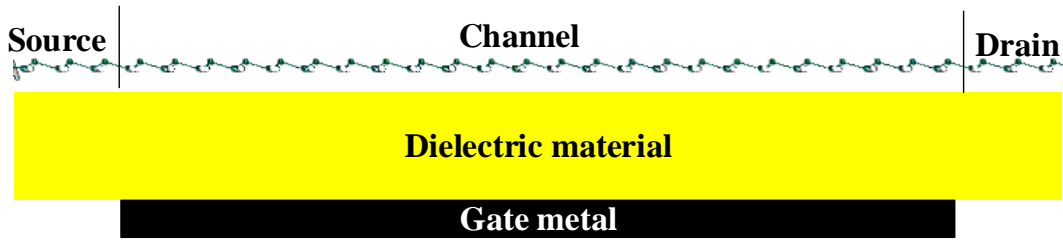
106 where $e, h, \Gamma, f_{L/R}$ and $\mu_{L/R}$ are electron charge, Planck's constant, contact broadening
 107 function of left(L) and right(R) electrodes, Fermi-Dirac distribution function of
 108 L/R electrodes and chemical potential of L/R electrode, respectively. Furthermore
 109 G is the Green's function of device that is given by:

$$G_d = (E - H_d - \Sigma_L - \Sigma_R)^{-1} \quad (2)$$

112 where E, H_d and $\Sigma_{L/R}$ are carrier energy, the Hamiltonian of device and the self-
 113 energy of L/R electrodes, respectively [40, 41]
 114

115

116



117

118

Fig2: Schematic of a simulated GeNR TFET

119

120

121 Fig. 2 shows the schematic of proposed GeNR-TFET. The p-i-n GeNR tunneling
 122 FET has a 10-nm long GeNR channel with index of $N=6$, where N is the number of
 123 atoms along the ribbon width. The gate insulators used in this study are $\text{SiO}_2(K=4)$
 124 and $\text{HfO}_2(K=25)$ with 1.5 nm thickness and the gate metal thickness is 0.5 nm. The
 125 source and drain lengths are the same and equal to 7.04 \AA . The gate insulator
 126 covers the entire nanoribbon but the gate metal only covers the channel. The
 127 channel is undoped whereas p-type and n-type dopants are introduced into the
 128 source and drain regions, respectively. Doping value is chosen 0.8%.

129 The utilized power supply voltage is $V_D=0.5V$. Lengths of the gate (L_{gate}) and
 130 channel are the same. L_{underlap} is considered from the edge of the gate to the junction
 131 of the drain.

132

133

134 3. Results and discussion

135 In this section the results obtained from the simulation of the device under study at
136 room temperature are discussed. Therefore, the transfer characteristics for hetero-
137 dielectric gate material, gate-drain underlap and hetero-junction at the source
138 region are presented. Their performance has been investigated in terms of ON-state
139 (I_{ON}) and ambipolar current (I_{amb}).

140 3.1. Impact of mono/hetero dielectric materials on the transfer characteristics

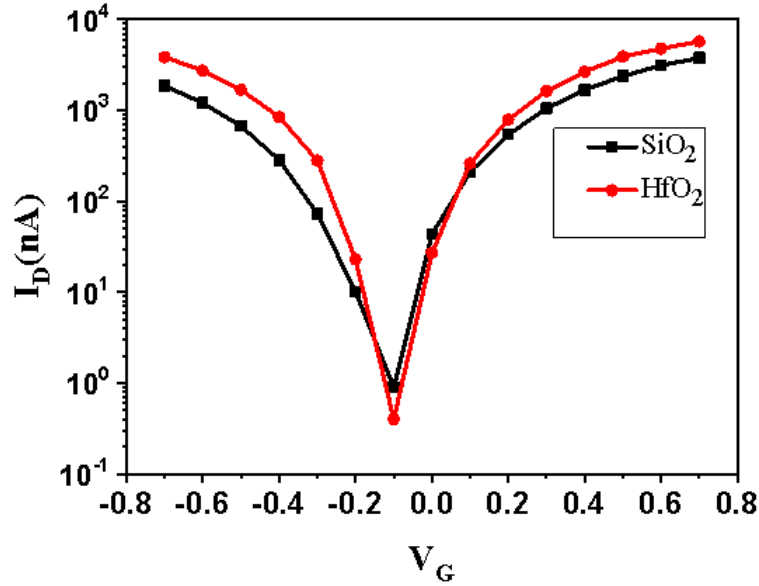
141 In this subsection, impact of hetero dielectric gate on controlling the ambipolar
142 characteristic is studied. In order to examine the obtained data, a detailed review on
143 the formulation of the tunnel current is required. The dependence of the ON state
144 current (I_{ON}) on the transmission probability in TFETs[35, 36] is explained by:

$$145 I \propto T(E) = \exp\left(-\frac{4\sqrt{2}m^*E^{\frac{3}{2}}}{3|e|\hbar(E_g+\Delta\varphi)}\sqrt{\frac{\epsilon_s}{\epsilon_{ox}}t_{ox}t_s}\right)\Delta\varphi \quad (3)$$

147 where e , \hbar , E_g , m^* and $\Delta\varphi$ represent the electron charge, the reduced Planck's
148 constant, the bandgap, the effective mass and the energy range of tunneling
149 location, respectively. t_{ox} and ϵ_{ox} are oxide thickness and dielectric constant while
150 t_s and ϵ_s denote the corresponding values for the semiconductor close to the tunnel
151 junction.
152

153 This equation indicates that ON-state current (I_{ON}) can be increased by increasing
154 the dielectric constant (ϵ_{ox}).The transfer characteristic (I_D - V_G) for the GeNR-TFET
155 presented in Fig. 2 was calculated for two different mono-dielectrics (SiO_2 and
156 HfO_2). The results obtained for this study are compared and shown in Fig. 3.

157

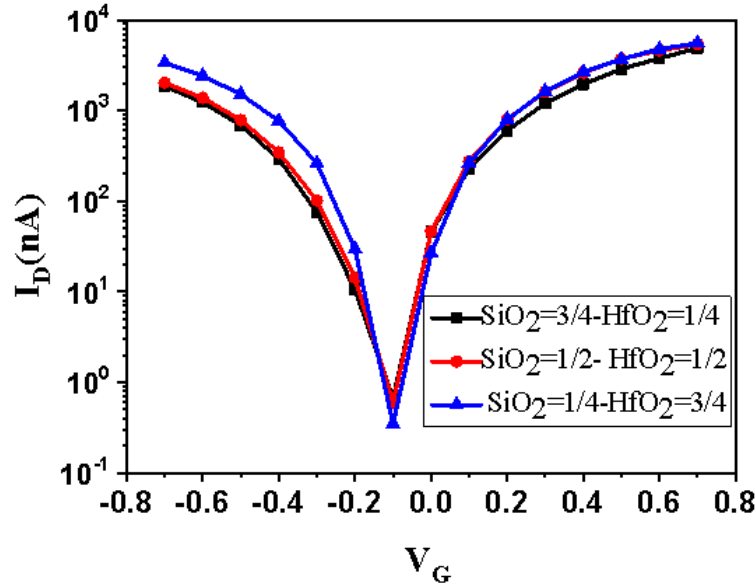


158
 159 **Fig. 3:** The current-voltage characteristics for two mono-dielectrics in GeNR-TFET under study
 160 at $V_{DS}= 0.5V$.
 161

162 Despite the improvement of the ON state and OFF-state (leakage) current for high-
 163 k dielectric case (HfO₂), Fig. 3 indicates that the ambipolar current in the GeNR-
 164 TFET utilizing HfO₂ dielectric is more. In order to overcome this problem, we
 165 examined the idea of using a different combination of high dielectric (HfO₂) and
 166 low dielectric (SiO₂) insulators at the source/drain sides of the channel. Fig.4
 167 compares the transfer characteristics at $V_D= 0.5V$ for the devices utilizing hetero-
 168 dielectric materials which is comprised of a combination of SiO₂ and HfO₂ in three
 169 cases:

- 170 a) Three-fourths of the dielectric length made from low-k material (SiO₂) and
 171 is located at the drain side and one-fourth of that made from high-k material
 172 (HfO₂) which is located at the source side.
- 173 b) Both sizes of high-k and low-k dielectrics are equal.
- 174 c) One-fourth of dielectric length made from SiO₂ and is located at the drain
 175 side and three-fourths of that made from HfO₂ which is located at the source
 176 side.

177 It is worth noting that in all three cases, high-k/ low-k materials are located close to
 178 the source/drain sides, respectively. In other words, the dielectric in the drain side
 179 is SiO₂ while the dielectric in the source side is HfO₂.



181
182 **Fig. 4:** The current-voltage characteristics for three cases of hetero-dielectric in GeNR-TFET
183 under study at $V_{ds} = 0.5V$.
184
185

186 According to Fig. 4, case *c* which utilizes more HfO_2 at the source side gives more
187 ON-state current (I_{ON}). This is in agreement with what we expect from equation 3
188 because occurrence of more tunneling necessitates use of high- k material in the
189 source side. Furthermore, the use of higher dielectric material with an increased
190 length leads to more electrostatic coupling between the gate and the junction of
191 source/channel resulting in the enhancement of I_{ON} .

192 As shown in Fig. 4, if the SiO_2 length becomes more than the length of the HfO_2
193 (case *a*) the ambipolar current decreases. However, it can be seen that I_{ON} is also
194 reduced, so there is a trade-off between the ambipolar current and I_{ON} .

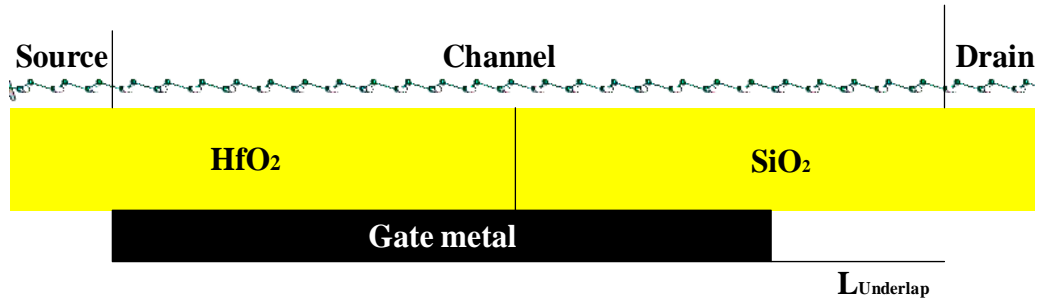
195 The sub-threshold swing (SS) is another important parameter of the field effect
196 transistor that is calculated as $SS = dV_G / d \log(I)$ [11]. It is desired to have a low SS
197 value, because it leads to better switching behavior of the transistor. It is worth
198 noting that since the drain current behavior of the tunneling devices is not linear
199 versus the gate voltage at the subthreshold region, the SS value must be measured
200 at a particular point and since the Dirac point has the highest slope, SS is
201 calculated at this point.

202 From Fig. 3 the calculated SS is equal to 54mV/decade for TFET utilizing SiO_2
203 and 50 mV/decade for the case utilizing HfO_2 . This indicates the use of high- k
204 material gives better or reduced value of SS for mono-dielectric case. However, for
205 hetero-dielectric cases shown in Fig.4, the SS value is between these two values

206 (50 and 54 mV/decade) and the more the length of high-k material, the less the
207 value of SS will be.

208 3.2. Impact of gate-drain underlap on the transfer characteristics

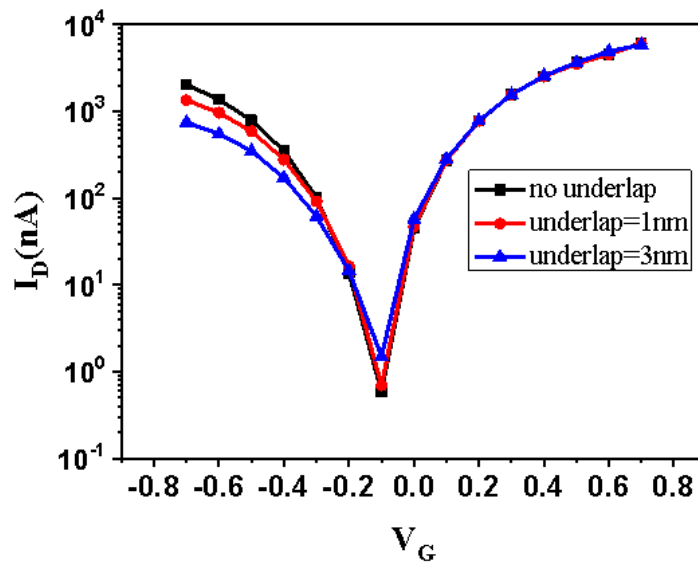
209
210 In this subsection, we would like to investigate the impact of gate underlap on the
211 ambipolar characteristic. In this study the channel length is fixed at 10 nm and the
212 gate underlap length is changed between 1 nm and 3 nm, as shown in Fig. 5.
213



214
215

216 **Fig. 5:** Schematic of GeNR-TFET with a gate-drain underlap.

217
218 Fig. 6 exhibits I-V characteristics for the GeNR-TFETs with various gate-drain
219 underlaps at $V_D = 0.5$ V. As shown in Fig. 6, ambipolar characteristic is suppressed
220 as the gate-drain underlap increases. In order to investigate the origin of this
221 observation the energy band diagram along the device length is plotted in Fig.7.
222



223

224 **Fig.6:** The current-voltage characteristics for various gate underlaps at the drain end of the
225 channel at $V_D = 0.5$ V.

226

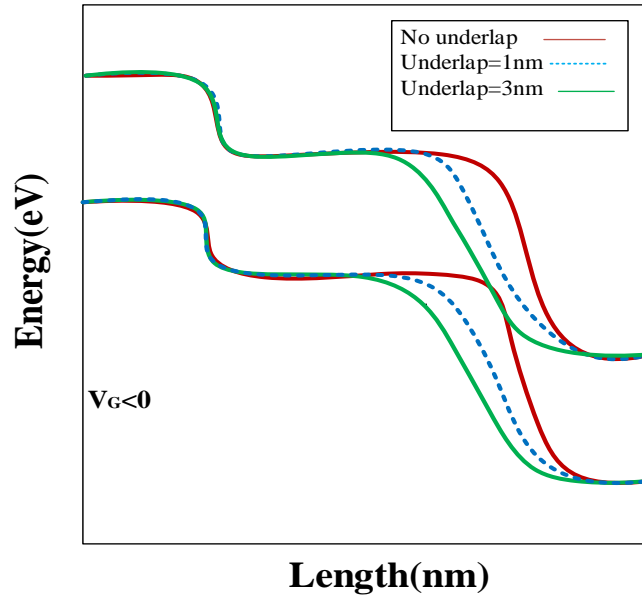


Fig.7: Band diagram in ambipolar state for different gate-drain underlaps.

228

229

230

231

232 It can be seen from Fig. 7 that the electric field generated by the gate voltage on
 233 the drain side gradually decreases as the gate underlap length increases. Due to
 234 reduction of the electric field at the drain-channel interface, the band bending is
 235 reduced and this in turn leads to an increase in the tunneling barrier width.
 236 Therefore, carrier tunneling in this interface is reduced. It is also observed that the
 237 gate-drain underlap does not have an effect on the source-channel interface.
 238 Therefore gate-drain underlap is one way of suppressing the ambipolar current.
 239 However, the length of the gate should not be so short, because by increasing the
 240 gate-drain underlap, direct current from source to drain increases and this might
 241 cause an unwanted increase in the drain current.

242 According to Fig.6, it can be seen that the when the length of the underlap is 1nm,
 243 it is optimum. This is due to the fact that the ambipolar current has decreased and
 244 the off-state current has not changed. Table 1 shows the electronic parameters of
 245 the device under study in comparison with other published works.

246

247

248

249

250

251

252

253

254
255
256
257
258
259

Table 1
Parameters of the optimal state of AGeNR-TFET Comparison of the main figures of merit of
TFETs made of several 2D channel materials.

parameter	This work	[42]	[11]	[43]
I_{ON}/I_{OFF}	10^4	1.9×10^3	10^5	-
SS (mV/decade)	52	68	11.54	-
Transconductance($gm \mu\Omega^{-1}$)(max)	14	-	11	-
DIBL	0.2 ($V_d=0.5V, V_g=1V$)	-	-	0.5

260
261
262
263

3.3. Impact of source bandgap on the transfer characteristics

264 Eventually, the device performance of a TFET composed of heterostructure
265 armchair GeNR (AGeNR) with a length of 10 nm and an index of $N=6$ for the
266 channel is evaluated. For AGeNR the band gap is determined by the width.
267 Considering the dependency between the width and band gap, AGeNRs are
268 classified into three groups: $N=3m$, $N=3m+1$ and $N=3m+2$; where N identifies the
269 number of germanium atoms along the ribbon width, and m is a positive integer. A
270 large, moderate and minimum band gap belong to $N=3m+1$, $N=3m$, and $N=3m+2$
271 groups, respectively. Due to strong dependence of the quantum confinement on the
272 nanoribbon width, for AGeNR, smaller band gaps are obtained with wider
273 ribbons[10, 44, 45]. Fig. 8 indicates the band structure of three germanene
274 nanoribbons with various widths of $N = 6, 8, 9$.

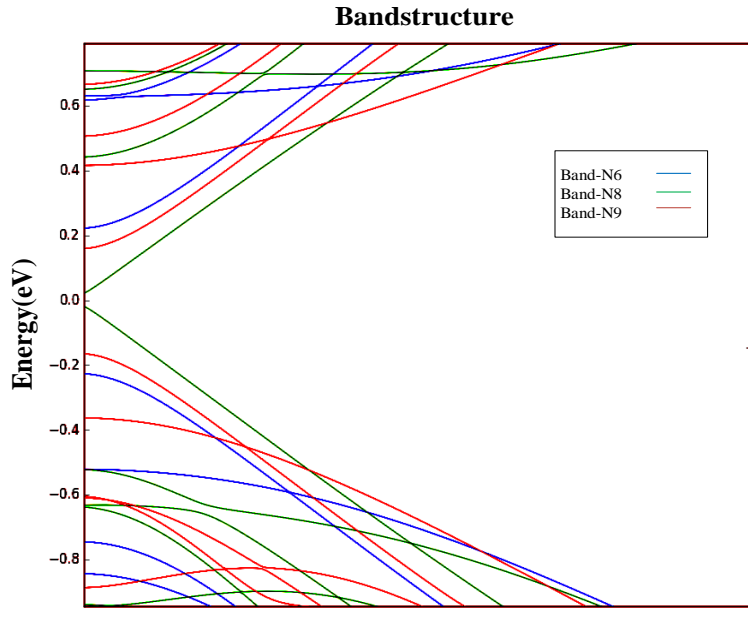


Fig.8: The band structure of three germanene nanoribbons with various widths of $N = 6, 8, 9$.

275
 276
 277
 278
 279
 280
 281
 282
 283
 284
 285
 286
 287

In order to better illustrate important electronic properties of AGeNRs, we extracted the electron effective mass and the bandgap from Fig.8. Fig. 9(a) shows variation in the effective mass with ribbon width (N) for the GeNRs with 6, 8 and 9 atoms along the width. As can be seen in Fig. 9(a), effective mass is changed depending on the width of the nanoribbon. Ribbon with width 6 has the highest effective mass and width 8 has the least effective mass among these three widths. Also in Fig.9 (b) variation in bandgap energy (E_g) versus ribbon width (N) is shown. As can be seen in Fig. 9(b), GeNR with width 6 has the highest band gap and width 8 has the lowest band gap among these three widths.

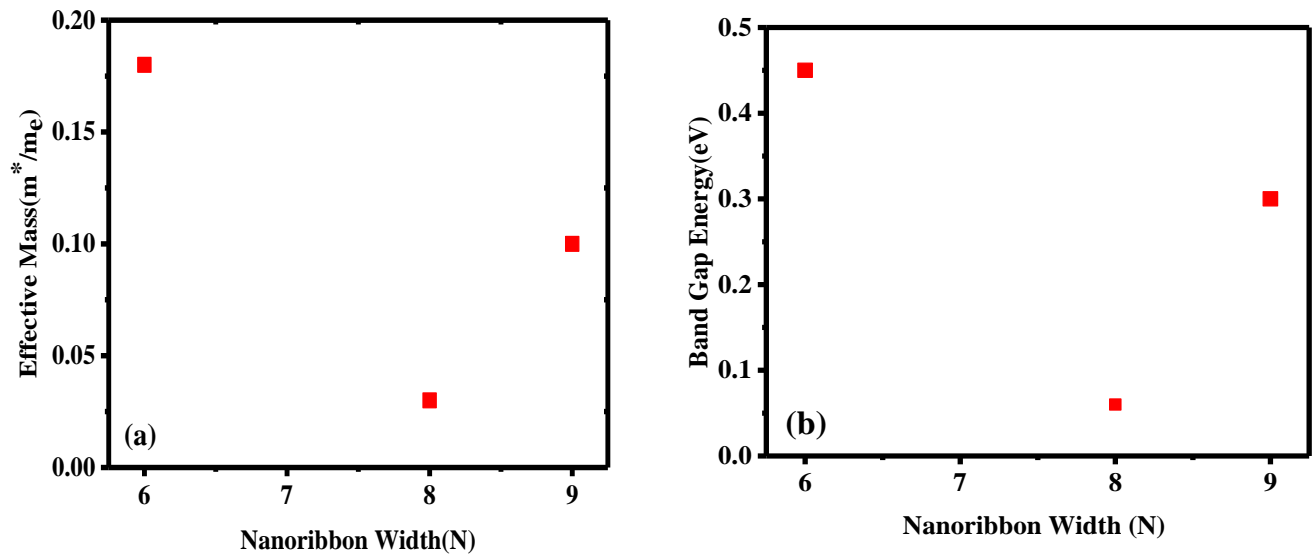
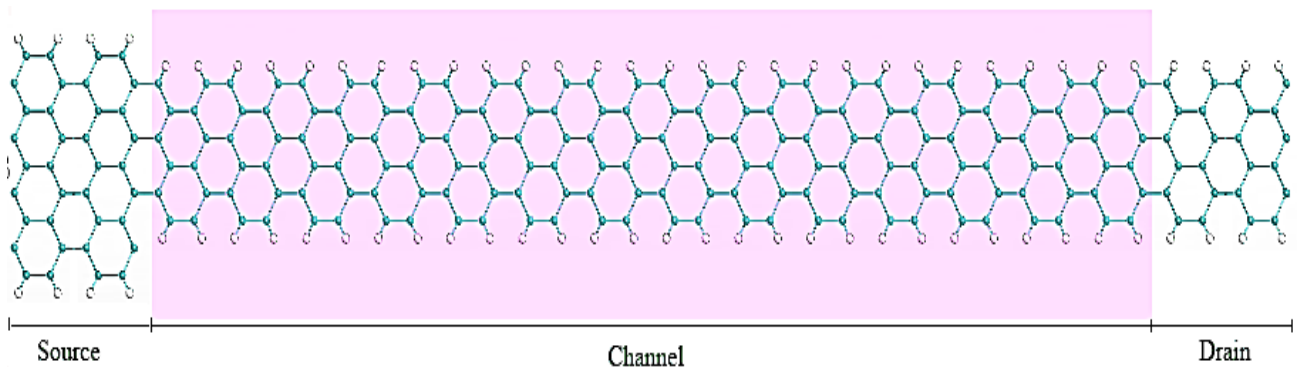


Fig.9: (a) The electron effective mass and (b) the bandgaps of GeNRs with different atoms along the width ($N = 6, 8, 9$).

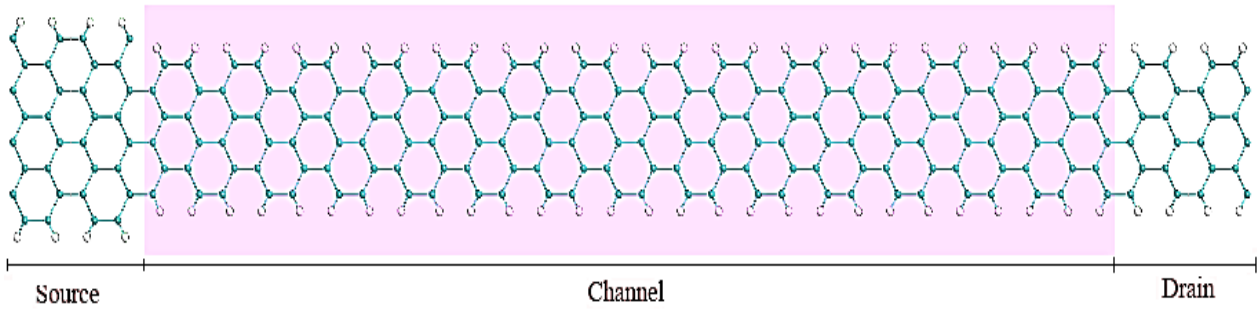
288

289 In these simulations, $N=8$ and $N=9$ in the source region are used because in these
 290 cases AGeNR behaves either metallic or semi-metallic. The case of $N=6$ is not
 291 suitable to be used in the source region because it shows a larger bandgap around
 292 0.4 eV as indicated in Fig. 8. The device atomic structure is shown in Fig.10.

293



294

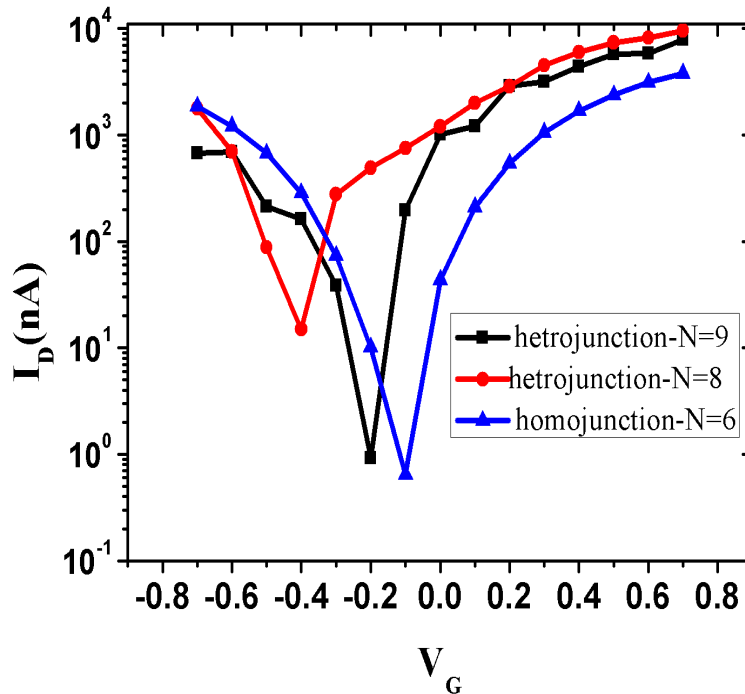


296

297 **Fig.10:** Atomic structure of simulated AGeNR-TFET with different widths in the source, top
 298 structure has N=9 atoms along the source width and bottom structure has N=8 atoms along the
 299 source width. The channel region is colored pink at the background.

300

301 The transfer characteristic for AGeNR-TFET with different configurations in the
 302 source is shown in Fig. 11. Three structures were simulated using first principles
 303 calculations comprised of (a)-homo-junction with N=6 for channel and source; (b)-
 304 hetero-junction with N=6 for channel and drain while N=8 for the source; (c)-
 305 hetero-junction with N=6 for channel and drain and N=9 for the source. From
 306 Fig.11, it is concluded that utilizing hetero-junctions at the source (small E_g) leads
 307 to higher I_{ON} but the I_{OFF} is increased compared with the homo-junction case. To
 308 explain the general transport mechanism of the GeNR-TFETs, energy band
 309 diagrams at OFF-state and ON-state are plotted in Fig. 12.



310

311 **Fig.11:** The current-voltage characteristics for GeNR-TFETs corresponding to N=6, 8 and 9 atoms along
 312 the source.

312

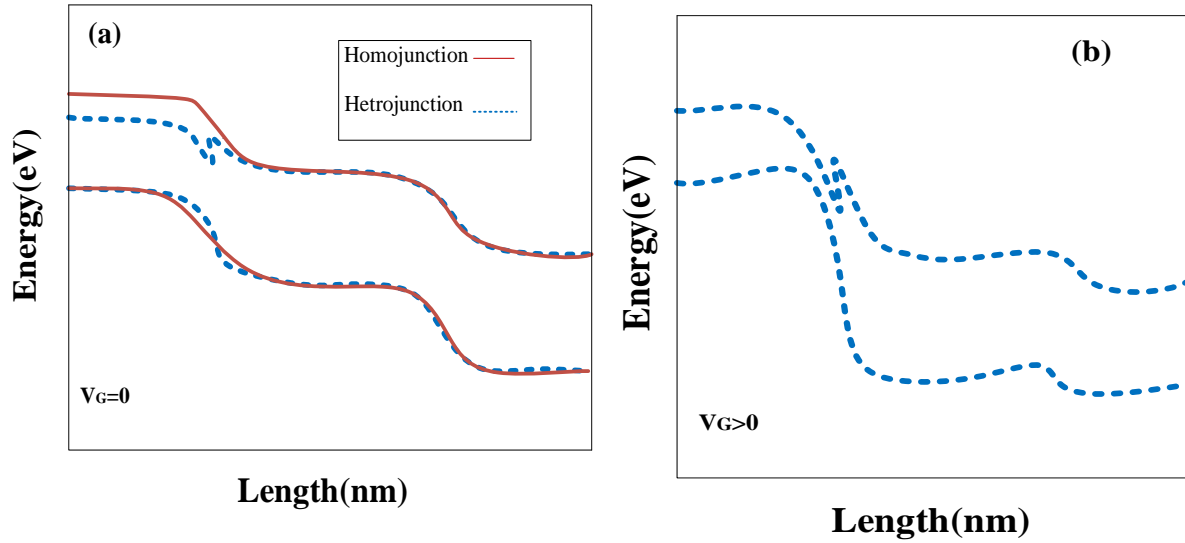


Fig.12: Energy band diagram for hetero-junction case at (a) OFF state and (b) ON state.

314

315

316

317 According to Fig. 12(a), at OFF-state the valence band of the source is located
 318 under the conduction band of the channel. Therefore, due to the lack of mobile
 319 carriers at the source/ drain-channel junctions, the major contributing of current is
 320 direct tunneling from source to drain. Using a smaller energy bandgap at the source
 321 reduces the effective tunneling width from the source to drain and as a result, I_{OFF}
 322 increases. Moreover, the ambipolar current has been improved, as shown in Fig.
 323 11.

324 Based on energy band diagram shown in Fig 12(b), at ON-state the valence band of
 325 the source is located upper than the conduction band of the channel. It can be seen
 326 that due to insertion of smaller E_G material in the source region, a sharper profile
 327 will be created in the source/channel junction and hetero-junction has a thinner
 328 tunneling barrier compared with homo-junction. As a result, the probability of
 329 carrier tunneling will be higher and the ON-state current becomes larger. Another
 330 factor in the improvement of ON-state current is the increase in tunneling area due
 331 to the presence of materials with smaller band gap in the source. This means that
 332 more electrons contribute to the band-to-band tunneling.

333 As a result, as the width of AGeNR in the source is increased, energy bandgap
 334 becomes smaller and the tunneling current increases. This is in agreement with the
 335 enhanced value of on-state current of hetero-junction with $N=8$ compared with on-
 336 state current of its counterpart having $N=9$. However, the ambipolar current will be
 337 worse in this case. Among these three cases, the overall behavior of the transfer

338 characteristic will be better for N=9 case, where the ambipolar current is one order
339 of magnitude less than the ON-state current as indicated in Fig. 11.

340

341 **Conclusion**

342 In this article, a back-gated GeNR tunneling field effect transistor is proposed and
343 its ambipolar current and ON-state current were theoretically studied. Due to the
344 undesirable effects of the ambipolar current on digital electronic applications, it
345 was shown that the use of hetero-dielectric material as well as a gate underlap
346 leads to improved performance of the device in terms of ambipolar current and
347 ON-state current. Moreover, performance of a GeNR-TFET with various hetero-
348 junctions in the source/channel interface was studied. Utilizing a wide ribbon with
349 smaller band gap in the source led to narrower tunneling width and an increase of
350 the tunneling area. Therefore, I_{ON} and ambipolar current were improved.

351 **Acknowledgements**

352 This research was supported by University of Kashan under supervision of
353 Dr.Daryoosh Dideban. Authors are thankful to the support received for this work
354 from Micoelectronics Lab (meLab) at the University of Glasgow, UK.

355 **References**

- 356 [1] E.-H. Toh, G. H. Wang, G. Samudra, and Y.-C. Yeo, "Device physics and design of germanium
357 tunneling field-effect transistor with source and drain engineering for low power and high
358 performance applications," *Journal of Applied Physics*, vol. 103, p. 104504, 2008.
- 359 [2] P. Zhao, J. Chauhan, and J. Guo, "Computational study of tunneling transistor based on graphene
360 nanoribbon," *Nano letters*, vol. 9, pp. 684-688, 2009.
- 361 [3] D. S. Yadav, D. Sharma, B. R. Raad, and V. Bajaj, "Impactful study of dual work function, underlap
362 and hetero gate dielectric on TFET with different drain doping profile for high frequency
363 performance estimation and optimization," *Superlattices and Microstructures*, vol. 96, pp. 36-
364 46, 2016.
- 365 [4] A. S. Verhulst, W. G. Vandenberghe, K. Maex, and G. Groeseneken, "Tunnel field-effect
366 transistor without gate-drain overlap," *Applied Physics Letters*, vol. 91, p. 053102, 2007.
- 367 [5] M. S. Sarker, M. M. Islam, M. N. K. Alam, and M. R. Islam, "Gate dielectric strength dependent
368 performance of CNT MOSFET and CNT TFET: A tight binding study," *Results in physics*, vol. 6, pp.
369 879-883, 2016.
- 370 [6] R. Huang, Q. Huang, S. Chen, C. Wu, J. Wang, X. An, et al., "High performance tunnel field-effect
371 transistor by gate and source engineering," *Nanotechnology*, vol. 25, p. 505201, 2014.
- 372 [7] G. Han, P. Guo, Y. Yang, L. Fan, Y. S. Yee, C. Zhan, et al., "Source engineering for tunnel field-
373 effect transistor: Elevated source with vertical silicon-germanium/germanium heterostructure,"
374 *Japanese Journal of Applied Physics*, vol. 50, p. 04DJ07, 2011.
- 375 [8] M. Zoghi, A. Y. Goharrizi, and M. Saremi, "Band gap tuning of armchair graphene nanoribbons by
376 using antidotes," *Journal of Electronic Materials*, vol. 46, pp. 340-346, 2017.

- 377 [9] C. Clendennen, N. Mori, and H. Tsuchiya, "Non-equilibrium Green function simulations of
378 graphene, silicene, and germanene nanoribbon field-effect transistors," *Journal of Advanced*
379 *Simulation in Science and Engineering*, vol. 2, pp. 171-177, 2015.
- 380 [10] M. Monshi, S. Aghaei, and I. Calizo, "Edge functionalized germanene nanoribbons: impact on
381 electronic and magnetic properties," *RSC Advances*, vol. 7, pp. 18900-18908, 2017.
- 382 [11] A. H. Bayani, D. Dideban, M. Vali, and N. Moezi, "Germanene nanoribbon tunneling field effect
383 transistor (GeNR-TFET) with a 10 nm channel length: analog performance, doping and
384 temperature effects," *Semiconductor Science and Technology*, vol. 31, p. 045009, 2016.
- 385 [12] H. Da, K.-T. Lam, G. S. Samudra, G. Liang, and S.-K. Chin, "Influence of contact doping on
386 graphene nanoribbon heterojunction tunneling field effect transistors," *Solid-State Electronics*,
387 vol. 77, pp. 51-55, 2012.
- 388 [13] A. Acun, L. Zhang, P. Bampoulis, M. Farmanbar, A. van Houselt, A. Rudenko, et al., "Germanene:
389 the germanium analogue of graphene," *Journal of physics: Condensed matter*, vol. 27, p.
390 443002, 2015.
- 391 [14] S. Trivedi, A. Srivastava, and R. Kurchania, "Silicene and germanene: a first principle study of
392 electronic structure and effect of hydrogenation-passivation," *Journal of Computational and*
393 *Theoretical Nanoscience*, vol. 11, pp. 781-788, 2014.
- 394 [15] S.-s. Li, C.-w. Zhang, W.-x. Ji, F. Li, P.-j. Wang, S.-j. Hu, et al., "Tunable electronic and magnetic
395 properties in germanene by alkali, alkaline-earth, group III and 3d transition metal atom
396 adsorption," *Physical Chemistry Chemical Physics*, vol. 16, pp. 15968-15978, 2014.
- 397 [16] Z. Ni, Q. Liu, K. Tang, J. Zheng, J. Zhou, R. Qin, et al., "Tunable bandgap in silicene and
398 germanene," *Nano letters*, vol. 12, pp. 113-118, 2011.
- 399 [17] T. P. Kaloni and U. Schwingenschlögl, "Stability of germanene under tensile strain," *Chemical*
400 *Physics Letters*, vol. 583, pp. 137-140, 2013.
- 401 [18] Y. Wang, J. Zheng, Z. Ni, R. Fei, Q. Liu, R. Quhe, et al., "Half-metallic silicene and germanene
402 nanoribbons: towards high-performance spintronics device," *Nano*, vol. 7, p. 1250037, 2012.
- 403 [19] S. Singh, K. Garg, A. Sareen, R. Mehla, and I. Kaur, "Doped armchair germanene nanoribbon
404 exhibiting negative differential resistance and analysing its nano-FET performance," *Organic*
405 *Electronics*, vol. 54, pp. 261-269, 2018.
- 406 [20] W. Zhang, C. Basaran, and T. Ragab, "Impact of geometry on transport properties of armchair
407 graphene nanoribbon heterojunction," *Carbon*, vol. 124, pp. 422-428, 2017.
- 408 [21] Y. Lv, Q. Huang, H. Wang, S. Chang, and J. He, "A numerical study on graphene nanoribbon
409 heterojunction dual-material gate tunnel FET," *IEEE electron device letters*, vol. 37, pp. 1354-
410 1357, 2016.
- 411 [22] Q. Zhang, T. Fang, H. Xing, A. Seabaugh, and D. Jena, "Graphene nanoribbon tunnel transistors,"
412 *IEEE Electron Device Letters*, vol. 29, pp. 1344-1346, 2008.
- 413 [23] A. Y. Goharrizi, M. Zoghi, and M. Saremi, "Armchair graphene nanoribbon resonant tunneling
414 diodes using antidote and BN doping," *IEEE Transactions on Electron Devices*, vol. 63, pp. 3761-
415 3768, 2016.
- 416 [24] M. Saremi, M. Saremi, H. Niazi, and A. Y. Goharrizi, "Modeling of lightly doped drain and source
417 graphene nanoribbon field effect transistors," *Superlattices and Microstructures*, vol. 60, pp. 67-
418 72, 2013.
- 419 [25] K. I. Bolotin, K. J. Sikes, Z. Jiang, M. Klima, G. Fudenberg, J. Hone, et al., "Ultrahigh electron
420 mobility in suspended graphene," *Solid State Communications*, vol. 146, pp. 351-355, 2008.
- 421 [26] P. Zomer, S. Dash, N. Tombros, and B. Van Wees, "A transfer technique for high mobility
422 graphene devices on commercially available hexagonal boron nitride," *Applied Physics Letters*,
423 vol. 99, p. 232104, 2011.

- 424 [27] K. S. Novoselov, A. K. Geim, S. Morozov, D. Jiang, M. I. Katsnelson, I. Grigorieva, *et al.*, "Two-
425 dimensional gas of massless Dirac fermions in graphene," *nature*, vol. 438, p. 197, 2005.
- 426 [28] S. Sahay and M. J. Kumar, "Controlling the drain side tunneling width to reduce ambipolar
427 current in tunnel FETs using heterodielectric BOX," *IEEE Transactions on Electron Devices*, vol.
428 62, pp. 3882-3886, 2015.
- 429 [29] M. Madhini and G. Saini, "Heterojunction tunnel FET with Heterodielectric BOX," in *2016*
430 *International Conference on Communication and Signal Processing (ICCSP)*, 2016, pp. 1743-1746.
- 431 [30] W. Li, H. Liu, S. Wang, S. Chen, and Z. Yang, "Design of high performance Si/SiGe heterojunction
432 tunneling FETs with a T-shaped gate," *Nanoscale research letters*, vol. 12, p. 198, 2017.
- 433 [31] D. B. Abdi and M. J. Kumar, "Controlling ambipolar current in tunneling FETs using overlapping
434 gate-on-drain," *IEEE Journal of the Electron Devices Society*, vol. 2, pp. 187-190, 2014.
- 435 [32] G. Lee, J.-S. Jang, and W. Y. Choi, "Dual-dielectric-constant spacer hetero-gate-dielectric
436 tunneling field-effect transistors," *Semiconductor Science and Technology*, vol. 28, p. 052001,
437 2013.
- 438 [33] J. S. Lee, J. H. Seo, S. Cho, J.-H. Lee, S.-W. Kang, J.-H. Bae, *et al.*, "Simulation study on effect of
439 drain underlap in gate-all-around tunneling field-effect transistors," *Current Applied Physics*, vol.
440 13, pp. 1143-1149, 2013.
- 441 [34] K. Nigam, S. Gupta, S. Pandey, P. Kondekar, and D. Sharma, "Controlling the ambipolarity and
442 improvement of RF performance using Gaussian Drain Doped TFET," *International Journal of*
443 *Electronics*, vol. 105, pp. 806-816, 2018.
- 444 [35] R. Goswami and B. Bhowmick, "Hetero-gate-dielectric gate-drain underlap nanoscale TFET with
445 a δp^+ Si $1-x$ Ge x layer at source-channel tunnel junction," in *2014 International Conference on*
446 *Green Computing Communication and Electrical Engineering (ICGCEE)*, 2014, pp. 1-5.
- 447 [36] P. Jain, V. Prabhat, and B. Ghosh, "Dual metal-double gate tunnel field effect transistor with
448 mono/hetero dielectric gate material," *Journal of computational electronics*, vol. 14, pp. 537-
449 542, 2015.
- 450 [37] *VNL-ATK is a licensed software which can be accessed from:*
451 *<https://docs.quantumwise.com/v2016/>.*
- 452 [38] Q. Pang, Y. Zhang, J.-M. Zhang, V. Ji, and K.-W. Xu, "Electronic and magnetic properties of
453 pristine and chemically functionalized germanene nanoribbons," *Nanoscale*, vol. 3, pp. 4330-
454 4338, 2011.
- 455 [39] M. Ali, X. Pi, Y. Liu, and D. Yang, "Electronic and magnetic properties of graphene, silicene and
456 germanene with varying vacancy concentration," *AIP Advances*, vol. 7, p. 045308, 2017.
- 457 [40] P. Sharma, S. Singh, S. Gupta, and I. Kaur, "Modeling linearity and ambipolarity in GFETs on
458 different dielectrics for communication applications," *Journal of Materials Science: Materials in*
459 *Electronics*, vol. 29, pp. 2883-2889, 2018.
- 460 [41] S. Chang, Y. Zhang, Q. Huang, H. Wang, and G. Wang, "Effects of vacancy defects on graphene
461 nanoribbon field effect transistor," *Micro & Nano Letters*, vol. 8, pp. 816-821, 2013.
- 462 [42] L. De Michielis, L. Lattanzio, K. E. Moselund, H. Riel, and A. M. Ionescu, "Tunneling and
463 occupancy probabilities: How do they affect tunnel-FET behavior?," *IEEE Electron Device Letters*,
464 vol. 34, pp. 726-728, 2013.
- 465 [43] L. Liu, D. Mohata, and S. Datta, "Scaling length theory of double-gate interband tunnel field-
466 effect transistors," *IEEE Transactions on Electron Devices*, vol. 59, pp. 902-908, 2012.
- 467 [44] S. Kaneko, H. Tsuchiya, Y. Kamakura, N. Mori, and M. Ogawa, "Theoretical performance
468 estimation of silicene, germanene, and graphene nanoribbon field-effect transistors under
469 ballistic transport," *Applied Physics Express*, vol. 7, p. 035102, 2014.
- 470 [45] D. Dideban, A. Ketabi, M. Vali, A. H. Bayani, and H. Heidari, "Tuning the analog and digital
471 performance of Germanene nanoribbon field effect transistors with engineering the width and

472 geometry of source, channel and drain region in the ballistic regime," *Materials Science in*
473 *Semiconductor Processing*, vol. 80, pp. 18-23, 2018.

474